Kar3Vik1, a member of the Kinesin-14 superfamily, shows a novel kinesin microtubule binding pattern

Katherine C. Rank,[1] Chun Ju Chen,[2] Julia Cope,[3] Ken Porche,[2] Andreas Hoenger,[3] Susan P. Gilbert,[2] and Ivan Rayment[1]

[1]Department of Biochemistry, University of Wisconsin, Madison, WI 53706
[2]Department of Biology and the Center for Biotechnology and Interdisciplinary Studies, Rensselaer Polytechnic Institute, Troy, NY 12180
[3]Department of Molecular, Cellular, and Developmental Biology, University of Colorado, Boulder, CO 80309

Kinesin-14 motors generate microtubule minus-end–directed force used in mitosis and meiosis. These motors are dimeric and operate with a nonprocessive powerstroke mechanism, but the role of the second head in motility has been unclear. In *Saccharomyces cerevisiae*, the Kinesin-14 Kar3 forms a heterodimer with either Vik1 or Cik1. Vik1 contains a motor homology domain that retains microtubule binding properties but lacks a nucleotide binding site. In this case, both heads are implicated in motility. Here, we show through structural determination of a C-terminal heterodimeric Kar3Vik1, electron microscopy, equilibrium binding, and motility that at the start of the cycle, Kar3Vik1 binds to or occludes two αβ-tubulin subunits on adjacent protofilaments. The cycle begins as Vik1 collides with the microtubule followed by Kar3 microtubule association and ADP release, thereby destabilizing the Vik1–microtubule interaction and positioning the motor for the start of the powerstroke. The results indicate that head–head communication is mediated through the adjoining coiled coil.

Introduction

A common theme of molecular motors is the dimeric motor domain. In processive kinesins, two heads typically allow for a hand-over-hand mechanism where one head is always bound to the microtubule, preventing dissociation (Svoboda et al., 1993; Hackney, 1994; Hoenger et al., 1998; Hancock and Howard, 1999; Asbury et al., 2003; Kaseda et al., 2003; Yildiz et al., 2004). Successful long-distance movement requires communication between the heads to synchronize stepping and prevent premature release from the microtubule. The molecular basis for this communication is not well understood but is thought to occur through chemical gating and strain in the neck linker (Rice et al., 1999; Yildiz et al., 2008; Clancy et al., 2011). A consequence of hand-over-hand motion is the introduction of asymmetry between the heads once bound to a microtubule such that a step by the right head is not equivalent to a step by the left head.

In contrast to the microtubule plus-end–directed processive motors, the Kinesin-14 motors are nonprocessive, minus-end–directed, and contain C-terminal motor domains connected by an N-terminal coiled coil (Vale and Fletterick, 1997; deCastro et al., 2000; Fink et al., 2009). They use a powerstroke mechanism involving rotation and bending of the coiled coil stalk toward the minus end of microtubules instead of a stepping mechanism (Wendt et al., 2002; Endres et al., 2006). Sequence analysis suggests that all motors in this class are dimeric. This raises the question of whether the second motor head of the Kinesin-14 dimer plays a direct role in motility.

Ncd, a well-studied homodimeric Kinesin-14 from *Drosophila melanogaster*, appears to display dramatic asymmetry between heads in solution studies (Foster et al., 1998, 2001; Foster and Gilbert, 2000). Ncd heterodimers have also been shown to promote motility with a single motor domain, prompting models where only one head is involved in the motile cycle (Wendt et al., 2002; Endres et al., 2006). However, studies of Ncd where mutations were introduced into one of the two motor

K.C. Rank and C.J. Chen contributed equally to this paper.

Correspondence to Susan Gilbert: sgilbert@rpi.edu; Andreas Hoenger: hoenger@Colorado.edu; or Ivan Rayment: ivan_rayment@biochem.wisc.edu

Abbreviations used in this paper: DPDPB, 1,4-di-[3′-(2′-pyridyldithio)propionamido]butane; EBI, *N,N′*-ethylenebis(iodoacetamide); M4M, 1,4-butanediyl bismethanethiosulfonate; RMSD, root mean squared deviation; SHD, synthetic heterodimer; TIRF, total internal reflection fluorescence; WT, wild type.

The Rockefeller University Press $30.00
J. Cell Biol. Vol. 197 No. 7 957–970
www.jcb.org/cgi/doi/10.1083/jcb.201201132

domains suggest that communication does occur between heads and is important for motility (Kocik et al., 2009). An even more dramatic example of this asymmetry is the Kinesin-14 heterodimer Kar3Vik1 from *Saccharomyces cerevisiae*. Here only Kar3 contains a motor domain, whereas Vik1 contains a motor homology domain (MHD) that binds to microtubules more tightly than the motor domain but lacks an ATP binding site (Allingham et al., 2007). This observation implies that both heads can participate in the motile cycle and that there must be communication between the two heads to allow Vik1 to dissociate from microtubules.

Kar3 is one of six kinesin motors found in *S. cerevisiae* (Meluh and Rose, 1990; Hildebrandt and Hoyt, 2000), and it functions as a heterodimer with either of the nonmotor proteins Vik1 or Cik1 (Page and Snyder, 1992; Page et al., 1994; Manning et al., 1999; Barrett et al., 2000). Kar3Vik1's biological function is to cross-link and stabilize parallel microtubules at the spindle pole body during mitosis (Manning et al., 1999). To accomplish this, the N-terminal section of Kar3Vik1 is thought to constitute an ATP-independent microtubule-binding domain connected by a long coiled coil to the C-terminal region, which contains the motor and MHDs. Kar3Cik1 is similarly organized, and it functions both in mitosis and meiosis to slide, stabilize, and depolymerize microtubules (Maddox et al., 2003; Chu et al., 2005; Sproul et al., 2005; Molk et al., 2006; Gardner et al., 2008). Mechanistic analysis suggests that Cik1, similar to Vik1, plays an active role in the motile cycle (Chen et al., 2011).

Previous studies of the Vik1MHD show that Vik1 contains a canonical kinesin fold despite lacking an ATP-binding site and binds to microtubules with a K_d of 43 ± 14 nM; this is in contrast to Kar3, which binds to microtubules with a K_d of 223 ± 26 nM in the ADP state and 119 ± 24 nM in the AMPPNP state (Allingham et al., 2007). These results demand that Vik1 binds to the microtubule and participates in the motile cycle. However, they do not provide evidence for when Vik1 participates in the motile cycle, how Vik1 binds to the microtubule, how the Kar3MD and Vik1MHD spatially relate to each other during the motile cycle, or whether Kar3Vik1 structurally resembles the homodimer Kinesin-14 motor Ncd.

A truncated heterodimer of Kar3Vik1 that displays wild-type (WT) activity was constructed to determine Kar3Vik1's mechanism of motion and to study the interactions between Kar3 and Vik1 (Fig. S1). Equilibrium binding and electron microscopy (EM) surface shadowing studies demonstrate that Kar3Vik1 has two distinct microtubule binding modes depending on the nucleotide state of Kar3. Kar3 and Vik1 bind to or interact with adjacent protofilaments in different orientations in the ADP and beginning of the nucleotide-free states. This is in contrast to the later nucleotide-free state and AMPPNP state where Kar3Vik1 binds only through Kar3. Uptake of AMPPNP causes a minus-end–directed rotation of the coiled coil, similar to Ncd's powerstroke mechanism (Wendt et al., 2002; Endres et al., 2006). A crystal structure of the Kar3Vik1 heterodimer and mechanistic analysis of a series of intra- and intermolecular cross-linked motors further support side-by-side binding of Kar3Vik1 at the beginning of the motile cycle. These results are consistent with a mechanism in which Kar3 binds to or occludes the microtubule lattice on an adjacent protofilament to Vik1, whereupon release of ADP from Kar3 allows for a transition to a Kar3-only bound state. Subsequently, ATP binding promotes the rotation of the coiled coil stalk toward the microtubule minus end.

Results

The previously described Kar3Vik1 heterodimer (Allingham et al., 2007) included an extended length of native coiled coil but was poorly behaved for large-scale purification. It exhibited limited solubility and was unsuitable for crystallization and EM. It was hypothesized that shortening the coiled coil would lead to better behaving protein; however, the coiled coil contains a low predicted coiled coil propensity adjacent to the globular domains. Hence, fusion constructs were created that included an N-terminal stable coiled coil either in the form of a GCN4 leucine zipper (O'Shea et al., 1991) or a synthetic heterodimer (SHD) containing an acidic and basic helix (Lindhout et al., 2004). Both SHD and GCN4 constructs retain two and a half heptads of native coiled coil sequence (Table 1 and Fig. S1). WT GCN4-Kar3Vik1 and WT SHD-Kar3Vik1 heterodimers promote robust microtubule minus-end–directed movement and exhibit ATPase properties consistent with their motility (Fig. S2, Video 1, and Video 4). Additional GCN4- and SHD-Kar3Vik1 motors were prepared that include inter- and intramolecular cross-links in a cysteine-free background (Table 1). Cross-linked motors were necessary for crystallization of Kar3Vik1 and provide insight into the conformational changes required for minus-end force generation.

Stoichiometry of binding during the motile cycle

A series of equilibrium binding experiments were pursued to determine whether the stoichiometry of WT GCN4-Kar3Vik1 binding to the microtubule lattice changed as a function of nucleotide state as seen for Kar3Cik1 (Chen et al., 2011). The results presented in Fig. 1 show that in the ADP and nucleotide-free states, WT GCN4-Kar3Vik1 binds to microtubule αβ-tubulin dimers at a stoichiometry of 1:2; i.e., saturation binding is achieved for 2 µM WT GCN4–Kar3Vik1 at 4 µM tubulin polymer. Because the Kar3•ADP state is weakly bound to the microtubule, it suggests that the ADP state, captured through these experiments, represents the initial collision complex, with Vik1 tightly bound to the microtubule and the Kar3•ADP head detached or weakly associated but obscuring a site on the microtubule lattice. These results are consistent with the EM surface metal shadowing (Fig. 2).

The nucleotide-free state for these experiments was achieved by preforming the MT•WT GCN4-Kar3Vik1 complex with ADP, followed by apyrase treatment to generate the nucleotide-free state. This most likely represents the order of events in vivo, where Kar3Vik1 binds first through Vik1 followed by Kar3 with ADP release. As such, the 1:2 nucleotide-free state seen here represents an intermediate that forms directly after microtubule collision and release of ADP from Kar3. It is thought that this initial nucleotide-free intermediate is bound to the microtubule through the Vik1MHD, with the Kar3MD either bound weakly to the microtubule or

Table 1. **Construct designs**

Construct name	Fusion	Mutations	Cross-link
WT GCN4-Kar3Vik1	GCN4		NA
Cysless GCN4-Kar3Vik1	GCN4	Kar3 (C391L, C469A, C517A, C566V, C655V) Vik1 (C377V, C436A, C536A, C596A, C640A)	NA
10 Å cross-linked GCN4-Kar3Vik1	GCN4	Kar3 (C391L, C469A, C517A, C566V, C655V, E382C) Vik1 (C377V, C436A, C536A, C596A,C640A, K372C)	M4M
20 Å cross-linked GCN4-Kar3Vik1	GCN4	Kar3 (C391L, C469A, C517A, C566V, C655V, E382C) Vik1 (C377V, C436A, C536A, C596A,C640A, K372C)	DPDPB
Non-cross-linked GCN4-Kar3Vik1	GCN4	Kar3 (C391L, C469A, C517A, C566V, C655V, E382C) Vik1 (C377V, C436A, C536A, C596A,C640A, K372C)	NA
WT SHD-Kar3Vik1	SHD		NA
Cysless SHD-Kar3Vik1	SHD	Kar3 (C391L, C469A, C517A, C566V, C655V) Vik1 (C377V, C436A, C536A, C596A, C640A)	NA
Non-cross-linked SHD-Kar3Vik1	SHD	Kar3 (C391L, C469A, C517A, C566V, C655V) Vik1 (C377V, C436A, C536A, C596A, C640A, E355C, K423C)	NA
Cross-linked SHD-Kar3Vik1	SHD	Kar3 (C391L, C469A, C517A, C566V, C655V) Vik1 (C377V, C436A, C536A, C596A, C640A, E355C, K423C)	EBI

A list of the composition of all constructs including the identity of the stabilizing coiled coil, mutations, and cross-links. Kar3 constructs included a Tobacco etch virus (TEV) protease cleavable His-tag with the sequence: *MGSSHHHHHHHHDYDIPTSENLYFQ*GASM followed by a fusion domain and K353-*K729* of Kar3. Vik1 constructs included a TEV protease cleavable Strep tag with the sequence *MASWSHPQFEKENLYFQ*GAS followed by a fusion domain and S341-*T647* of Vik1. Amino acids in italics were removed by TEV protease. The sequences of GCN4, basic helix, and acidic helix in the fusions were: SVKELEDKVEELLSKNYHLENEVARLKKLV, KIAALKEKIAALKEKIAALKEKI, and EIAALEKEIAALEKEIAALEKEI, respectively. For the SHD fusions, Kar3 was fused to the basic helix, and Vik1 to the acidic helix.

in close proximity to the microtubule lattice occluding binding by another Kar3Vik1.

The ATP state, generated by the nonhydrolyzable analogue AMPPNP, resulted in saturation binding at a 1:1 stoichiometry. These results indicate that Kar3 now occupies every αβ-tubulin subunit, and this can only occur if the Vik1MHD does not obscure the β-tubulin binding site of Kar3.

ADP induces a dimeric binding configuration of Kar3Vik1 on adjacent protofilaments

Unidirectional surface metal shadowing of WT GCN4-Kar3Vik1 bound to the surface of microtubules in the presence of ADP (Fig. 2) reveals configurations of dimers that are indicative of side-by-side binding of the two heads. With ADP present, the two heads seem to prefer interaction with adjacent protofilaments rather than along the same protofilament as found with dimeric Eg5 (Fig. 2, insets; see also Krzysiak et al., 2006). Although it is impossible to distinguish between the Kar3MD and Vik1MHD, the surface shadowing method produces a very clear picture of the dimeric arrangements of the motor complexes because of its high contrast and elimination of image information from densities below the surface. After counting the configurations that show a clear lateral interaction of the Kar3Vik1 heterodimer over two adjacent protofilaments versus an axial binding configuration, such as those predominantly found with motors like dimeric Eg5 constructs (Fig. 2 inset) and other processive kinesins (Skiniotis et al., 2003), ∼90% of the motors were observed to adopt a lateral binding conformation (82 lateral positions versus 8 axial). A small number of dimers appear to adopt a binding conformation seen with AMPPNP or nucleotide-free states in which one head is bound and one head is free; these motors have been denoted with white arrows in Fig. 2. The stochastic binding observed for the Kar3Vik1•ADP complex differs markedly from that of Kar3Vik1 in the nucleotide-free and AMPPNP states, which exhibit strong cooperative binding (Cope et al., 2010).

Unidirectional surface metal shadowing offers several advantages for this study, foremost of which is its ability to directly observe single-molecule events without averaging or other image enhancement techniques. In binding situations like the ones observed here, it is not possible to use helical or other averaging-based three-dimensional reconstruction methods, as the stochastic double-binding configuration of Kar3Vik1 in the ADP state can never fulfill the requirements for helical averaging, which requires that every αβ-tubulin interact with the same binding partner. Here, one Kar3Vik1 heterodimer interacts with two αβ-tubulin units in a random distribution on the microtubule lattice. Freeze-drying and surface shadowing does induce flattening of the microtubules, which brings the outer rims of the protofilaments into closer proximity than in a tube, as the lateral "hinges" between protofilaments are toward the inner side. Hence, this closes these gaps by ∼20%, or ∼1 nm. However, it seems very unlikely that this distortion of lateral protofilament spacing accounts for the observed binding to adjacent filaments, as 1:2 binding is also seen in solution (Fig. 1). Rather, the metal shadowing provides a visual confirmation of what is evident in solution and supported by the cross-linking studies that follow. Metal shadowing has previously produced images that strongly agree with cryo-EM on kinesin–microtubule complexes and solution phase studies (Krzysiak et al., 2006). Metal shadowing is not appropriate for investigating the interaction of the nucleotide-free and AMPPNP states for Kar3Vik1 because these exhibit cooperative binding and do not yield the sparse binding required for observation of single-molecule interactions. Thus, for these complexes, cryo-EM and helical averaging are the methods of choice, as described later.

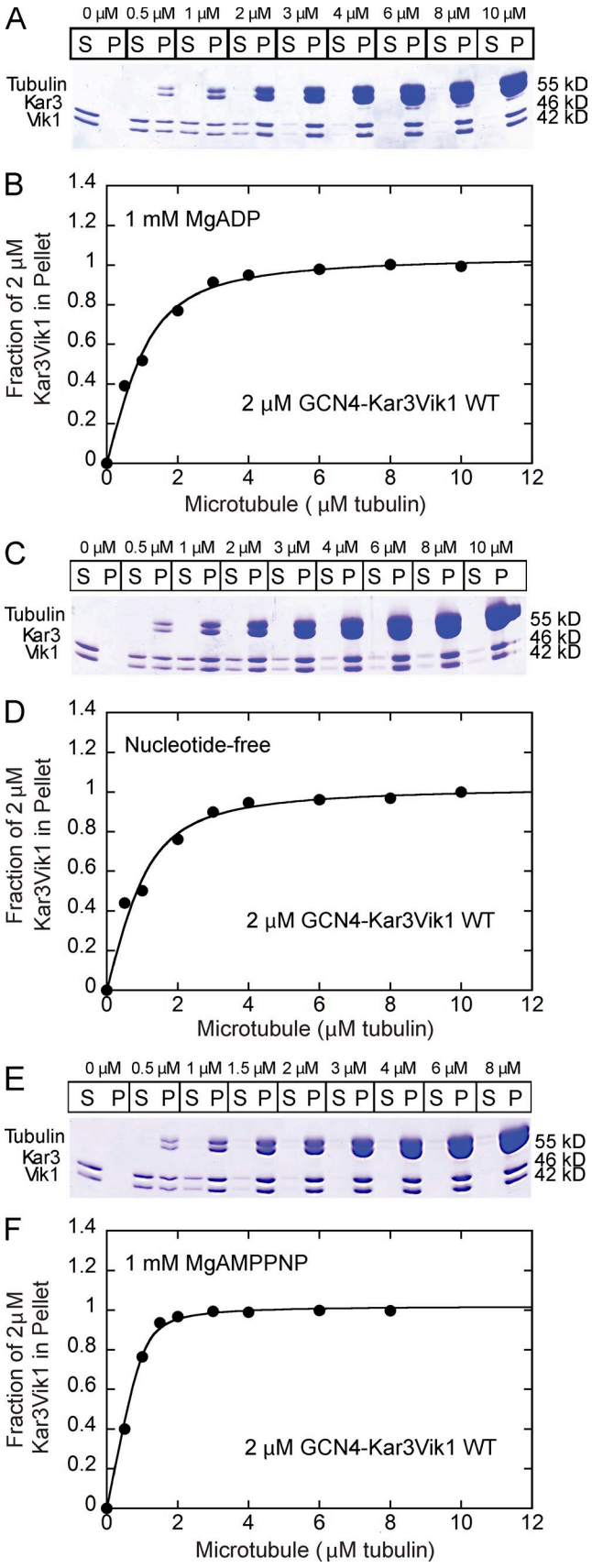

Figure 1. **Microtubule binding by WT GCN4-Kar3Vik1.** MT•Kar3Vik1 cosedimentation was performed to evaluate the binding properties based on the nucleotide state (A–F). 1 mM MgADP (A and B), 100 µM MgADP followed by apyrase treatment (C and D), and 1 mM MgAMPPNP (E and F). The supernatant (S) and pellet (P) for each reaction are shown with the gels, and the concentration of tubulin polymer is identified above each pair. The fraction of 2 µM WT GCN4-Kar3Vik1 that partitioned with MTs was plotted as a function of microtubule concentration. The fit of the data provided $K_{d,MT}$ = 0.37 ± 0.07 µM for ADP (B), n = 3; $K_{d,MT}$ = 0.36 ± 0.07 µM for nucleotide-free (D), n = 2; and $K_{d,MT}$ = 0.04 ± 0.01 µM for AMPPNP (F), n = 3, with all three at ∼100% maximal binding. The stoichiometry of WT GCN4-Kar3Vik1 binding to microtubules was 1:2 for ADP (B) and nucleotide-free states (D) (i.e., 2 µM Kar3Vik1 per 4 µM αβ-tubulin), and 1:1 for AMPPNP (F; i.e., 2 µM Kar3Vik1 per 2 µM αβ-tubulin). Numbers to the right of the gels indicate the experimentally derived molecular masses (in kilodaltons) of the proteins being analyzed. No molecular weight markers were run on these gels.

Structure of the Kar3Vik1 heterodimer

The structure of the Kar3Vik1 heterodimer was determined by x-ray crystallography to 2.3-Å resolution to establish the relationship between Kar3 and Vik1 (Fig. 3 A). This information cannot be deduced from the structures of the individual domains for Kar3 and Vik1 and is required to understand the communication between the two proteins. The structure contains the Kar3Vik1 heterodimer and reveals that the interface is formed by the adjoining N-terminal coiled coils. MgADP is bound to the active site of Kar3, as is observed in most structures of kinesin. The electron density for the secondary structural elements is well defined, although some loops within Vik1 are disordered, as is common for many microtubule-binding proteins. The Kar3MD and Vik1MHD show great similarity to previously solved structures. Kar3 has a root mean squared deviation (RMSD) of 0.89 Å for 300 structurally equivalent α-carbons, and Vik1 has a RMSD of 0.84 Å for 245 structurally equivalent α-carbons relative to the structures of the isolated domains (PDB accession nos. 3KAR and 2O0A; Gulick et al., 1998; Allingham et al., 2007). The structure displays the coiled coil registration that was predicted in the construct design (Figs. S1 and S3). The initial crystals diffracted exceedingly poorly (10-Å resolution). Crystal order was dramatically enhanced to 2.3-Å resolution by introducing an intramolecular cross-link within Vik1 as described later. It was also improved by replacing the GCN4 fusion with the shorter SHD domain and by systematically adjusting the freezing conditions. The original crystals of the WT heterodimer displayed the same crystal form as the cross-linked SHD Kar3Vik1; however, they only diffracted to 10-Å resolution, which was insufficient to determine if these crystals displayed the same unit cell and space group as those used in the structural determination presented here. Numerous other Kar3Vik1 motors were examined where cross-links were introduced at different locations within the heterodimer. These all crystallized with the same unit cell and space group but diffracted to a much lower resolution.

A symmetric 12-Å covalent cross-link was introduced between Vik1's helix (E355C) and globular domain (K423C) with the iodoacetamide based reagent *N*,*N*′-ethylenebis(iodoacetamide) (EBI) to improve crystal diffraction (Fig. 3 B). The location of the cross-link was chosen based on the orientation of the N-terminal α-helix in the Vik1MHD (Allingham et al., 2007). The cross-link itself is well defined within the structure. Motility analyses show that cross-linked SHD-Kar3Vik1 promoted microtubule gliding at 3.47 ± 0.03 µm/min compared with a rate of

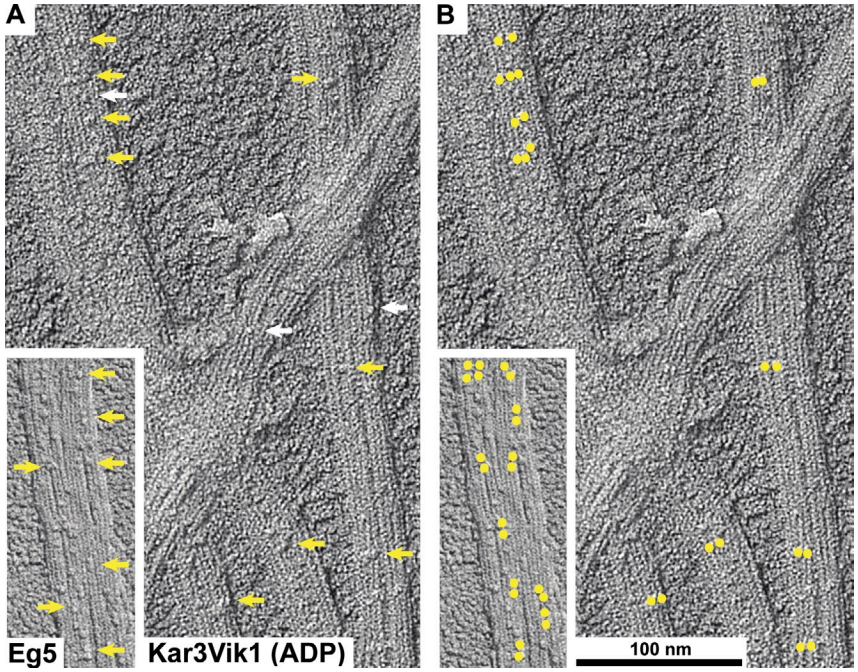

Figure 2. **High-resolution, unidirectional surface metal shadowing of WT GCN4-Kar3Vik1 bound to the surface of microtubules in the presence of ADP.** A and B are identical images with the dimeric motor domains indicated with yellow arrows in A, and directly marked with yellow dots in B. Examples of binding of Kar3Vik1 to the microtubule by a single head are indicated with white arrows. The dominant configuration of Kar3Vik1 crosses over two protofilaments. This is strikingly different from dimeric Eg5 (inset: AMPPNP), which predominantly binds with both heads along the same protofilament (see Krzysiak et al., 2006). Unlike other nucleotide states, cooperative binding is not observed. The scale for the insets is the same as in the main panels.

4.32 ± 0.04 µm/min for the non-cross-linked species (Fig. S2, and Videos 2 and 3). Retention of motility demonstrates that the protein used in the structural determination represents an active motor, and shows that, in contrast to Kar3, rotation of the coiled coil relative to Vik1 is not needed for the powerstroke.

Crystal structures of the Ncd dimer show two general conformations. In the first structure, the two heads are symmetrically related by a twofold axis coincident with the coiled coil, PDB accession no. 2NCD (Sablin et al., 1998). It is likely that the symmetrical crystal structure represents a solution phase conformation because binding to microtubules introduces asymmetry between the heads, as seen by EM (Sosa et al., 1997; Hirose et al., 1998; Wendt et al., 2002; Endres et al., 2006). In subsequent crystallographic structures of mutant Ncd dimers (Fig. 3 C), one head (head A) is in a conformation similar to the symmetric structure of Ncd, whereas the other (head B) is rotated relative to the coiled coil by ~70° (PDB accession nos. 3L1C and 1N6M; Yun et al., 2003; Heuston et al., 2010).

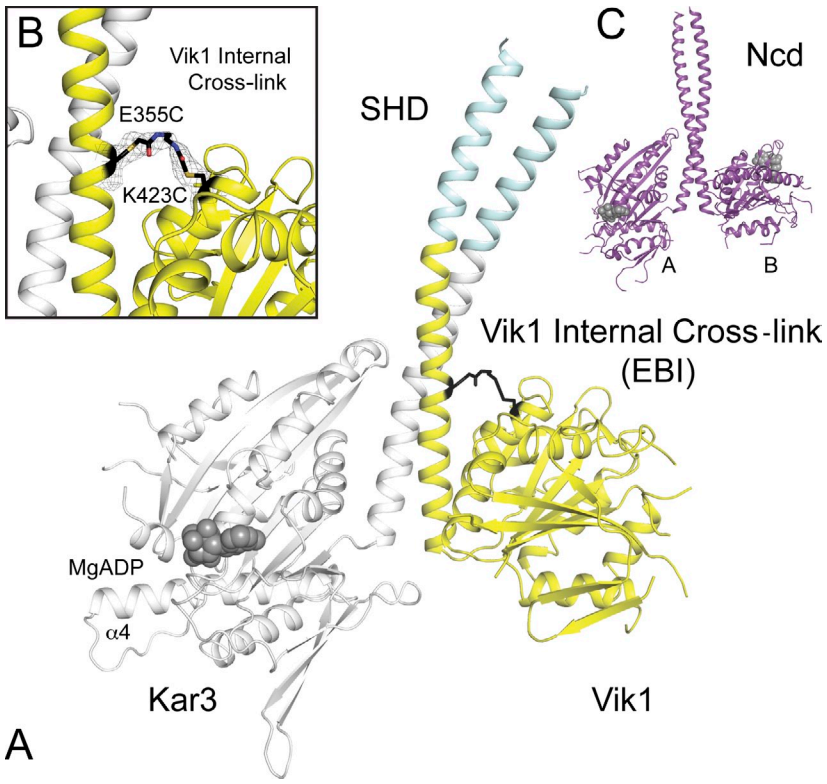

Figure 3. **Structure of cross-linked SHD-Kar3Vik1 and comparison to Ncd.** (A) A ribbon representation of the structure of cross-linked SHD-Kar3Vik1 (PDB accession no. 4ETP) solved to a resolution of 2.3 Å by x-ray crystallography, where the SHD is shown in pale cyan, Vik1 in yellow, and Kar3 in white. Kar3 is complexed to MgADP, which is shown in the space filling representation. Kar3's helix α4 is denoted as a point of reference. (B) Vik1 contains a 12-Å intramolecular cross-link (EBI) between its globular domain (K423C) and helix (E355C). Electron density for the cross-link is shown at a contour level of 1σ. (C) The structure of cross-linked SHD-Kar3Vik1 shows striking similarity to the asymmetric structures of Ncd (PDB accession nos. 1N6M and 3L1C; Yun et al., 2003; Heuston et al., 2010). The active sites of Ncd contain MgADP, shown in space filling representation. Fig. 3 was prepared with Pymol.

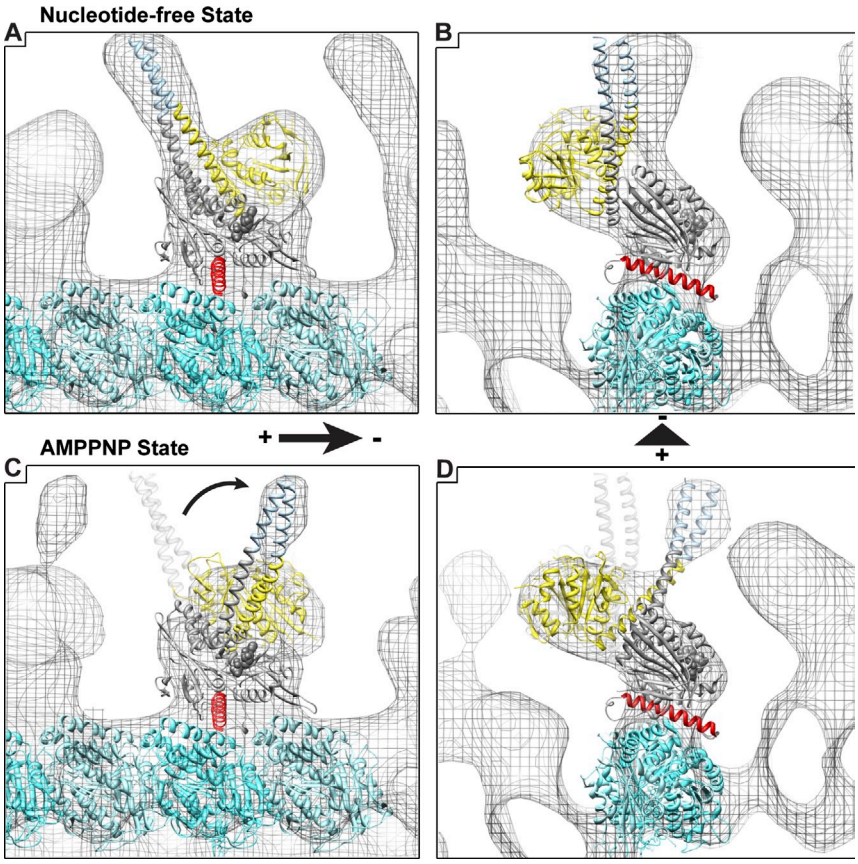

Figure 4. **Docking of the Kar3Vik1 crystal structure to the cryo-EM data.** Docking of the cross-linked SHD-Kar3Vik1 crystal structure into the three-dimensional maps obtained from helical reconstruction of WT GCN4-Kar3Vik1–decorated microtubules in the nucleotide-free (A and B) and AMPPNP (C and D) states. A and C show views along the length of the protofilament, with the minus end of the microtubule pointing to the right. B and D provide views through the cross section of the microtubule with the minus end facing away from the reader. Kar3, Vik1, the SHD domain, α-tubulin, and β-tubulin are depicted in gray, yellow, pale blue, light turquoise, and dark turquoise, respectively. Helix α4 of Kar3 is depicted in red in all the maps to orient the reader. In C and D, the docked position of Kar3Vik1 in the nucleotide-free state is shown in transparent gray.

The structure of Kar3Vik1 shows surprising similarity to the asymmetric Ncd structures, where Kar3's position relative to the coiled coil is similar to head A and Vik1 is rotated relative to the coiled coil by ∼70°, similar to head B. Alignment of Kar3Vik1 to dimeric Ncd (PDB accession no. 1N6M) gives an RMSD of 2.6 Å for 492 structurally equivalent α-carbons that extend across both heads of Ncd and Kar3Vik1. This is remarkable considering that Vik1 displays only 12% sequence identity and 20% sequence similarity to Ncd, lacks ATP binding capabilities, and displays different microtubule binding affinities and regulation compared with Ncd. The structural similarity supports the assertion that the conformation seen in both the asymmetric structure of Ncd and the structure of Kar3Vik1 presented here represents a biologically important and structurally conserved conformation, despite the orientation of Vik1 relative to the coiled coil being constrained by the introduced cross-link. This is further supported by the robust motility of cross-linked SHD-Kar3Vik1. Cryo-EM of WT motors indicates that the structure of Kar3Vik1 seen here represents the pre-powerstroke position, not the post-powerstroke position, as was suggested for the conformationally equivalent Ncd structures (Fig. 4; Yun et al., 2003).

Docking of the Kar3Vik1 crystal structure into WT GCN4-Kar3Vik1 cryo-EM maps

Cryo-EM and subsequent helical reconstruction of WT GCN4-Kar3Vik1 complexed to microtubules in the nucleotide-free and AMPPNP states (Fig. 4) revealed maps that closely resemble the cryo-EM maps of Ncd complexed to microtubules, once again illustrating the similarity in the powerstroke between these two related motors (Wendt et al., 2002; Endres et al., 2006). Highly similar cryo-EM maps were also obtained from cross-linked mutants, demonstrating that none of the cross-links prevent rotation of the coiled coil (Fig. S4). For both the nucleotide-free and AMPPNP states, the cross-linked SHD-Kar3Vik1 crystal structure was treated as a rigid body, and the docking was performed manually by aligning the orientation of the Kar3MD with respect to the microtubule protofilament according to the conformation published previously (Hirose et al., 2006). This conformation is very close to docking attempts reported for the microtubule-bound heads of Ncd (Sosa et al., 1997) and Kinesin-1 (Hoenger et al., 1998). Hence, the Kar3MD binds with the nucleotide binding site facing away from the microtubule surface and toward the microtubule minus end, with the neck coiled coil pointing toward the microtubule plus end.

The crystal structure fits extremely well into the map of WT GCN4-Kar3Vik1 complexed to microtubules in the nucleotide-free state, reinforcing the claim that the Kar3Vik1 x-ray structure represents a biologically relevant pre-powerstroke conformation (Fig. 4, A and B). This marked structural agreement also confirms that the microtubule minus-end–directed powerstroke is unlikely to occur when ADP is released from the active site upon microtubule binding, as has been proposed previously (Yun et al., 2003; Hirose et al., 2006), and instead takes place upon uptake of ATP.

Docking of the cross-linked SHD-Kar3Vik1 crystal structure into the map of the AMPPNP state shows that the interactions

between the coiled coil stalk and Kar3, as found in the crystal structure as well as in the nucleotide-free state in the EM three-dimensional maps, must change upon uptake of ATP, whereas the interactions between the stalk and Vik1 remain largely intact at the resolution of the EM. To fit Kar3Vik1 into the AMPPNP state map, the heterodimer was separated into two components: the Kar3MD core (residues G385-K729) and the complete Vik1MHD with the coiled coil stalk. The docking of the Kar3 core domain into the maps of the AMPPNP state remained almost unchanged compared with the nucleotide-free state, which indicates that only a slight rotation of Kar3 occurs during uptake of ATP and the powerstroke (Fig. 4, C and D), as has been described previously (Hirose et al., 2006). The small changes in Kar3's nucleotide-binding pocket are transmitted into a large structural rearrangement of Vik1 and the coiled coil stalk to position the stalk toward the minus end of the microtubule. Vik1 and the stalk had to be rotated at G385 on Kar3 by ~90° around an axis perpendicular to the coiled coil to fit optimally into the electron density map; this is consistent with the range of 70–90° observed for Ncd (Wendt et al., 2002; Endres et al., 2006). This close fit was obtained by rotating Vik1 and the stalk as a rigid body, which is consistent with the concept that contacts between the coiled coil and Vik1's core remain intact during the powerstroke.

The exclusive binding of the Kar3MD in the nucleotide-free state seen by cryo-EM does not reflect the binding of both the Kar3MD and Vik1MHD seen by equilibrium binding. It is likely that this is caused by differences in sample preparation. In the equilibrium binding experiments, Kar3Vik1 was bound to microtubules in the ADP form, which shows 1:2 binding, then treated by apyrase to generate the nucleotide-free state (Fig. 1). In contrast, successful helical reconstruction required the protein to be incubated with apyrase in solution and then bound to microtubules. In the latter case, the absence of nucleotide from the motor domain favors strong cooperative binding of Kar3 directly to the microtubule. Repetition of equilibrium binding experiments where Kar3Vik1 is first treated with apyrase and then bound to microtubules shows a clear shift in binding equilibrium toward 1:1 binding (Fig. 5).

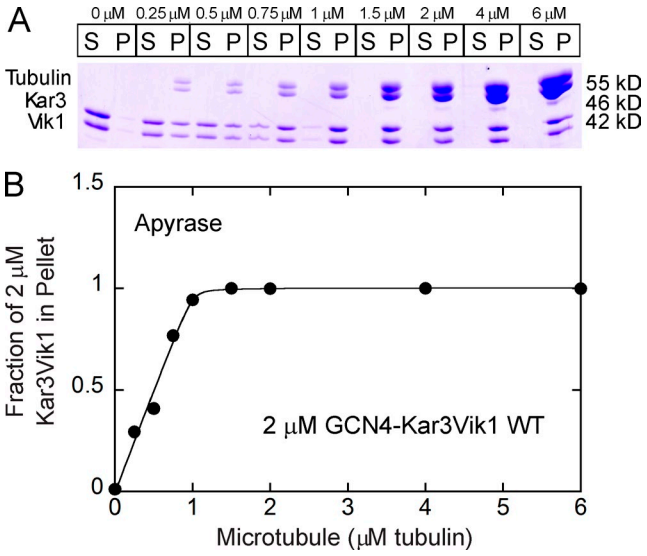

Figure 5. **Microtubule binding by nucleotide-free WT GCN4-Kar3Vik1.** Kar3Vik1 was treated with apyrase to generate nucleotide-free Kar3Vik1 and then mixed with microtubules. The resulting MT•Kar3Vik1 complex was evaluated by sedimentation to determine the binding properties of this intermediate. (A) The supernatant (S) and pellet (P) for each reaction are shown with the gel, and the concentration of tubulin polymer is identified above each pair. (B) The fraction of 2 μM apyrase-treated Kar3Vik1 that partitioned with microtubules was plotted as a function of microtubule concentration. The data shown are from a single representative experiment. The fit of the data provided the apparent $K_{d,MT}$ for each experiment with the mean ± SEM, $K_{d,MT}$ = 0.003 ± 0.004 μM, n = 2. The stoichiometry of binding is somewhat less than 1:1; i.e., 2 μM Kar3Vik1 binds to ~1.5 μM αβ-tubulin. Numbers to the right of the gels indicate the experimentally derived molecular weights (in kilodaltons) of the proteins being analyzed. No molecular weight markers were run on these gels.

Kar3Vik1 binds the microtubule lattice on two sites located on adjacent protofilaments

Metal shadowing of WT GCN4-Kar3Vik1 displayed interaction of the Kar3 and Vik1 heads with two adjacent protofilaments. This novel kinesin binding pattern was confirmed by introducing cross-links at the base of Kar3Vik1's coiled coil between Kar3 E382C and Vik1 K372C, using 1,4-butanediyl bismethanethiosulfonate (M4M) to generate a 10-Å cross-link as well as 1,4-di-[3′-(2′-pyridyldithio)propionamido]butane (DPDPB) to generate a 20-Å cross-link, restricting the distance of separation that can occur between the Kar3 and Vik1 heads (Fig. 6, A and B; and Table 1). The nonreducing gel in Fig. S5 shows >99% cross-linking efficiency for both M4M and DPDPB, which indicates that both populations of cross-linked GCN4-Kar3Vik1 motors are homogenous. The β-carbons of Kar3 E382C and Vik1 K372C are 10.9-Å apart, which is consistent with a coiled coil. Introduction of the 10-Å M4M cross-link therefore permits only a small movement between these residues, whereas the 20-Å DPDPB cross-link potentially allows an additional 10 Å of movement. Most importantly, neither the M4M nor DPDPB cross-link allows for enough separation for both heads to interact with the same protofilament, which would require ~80 Å of separation.

Microtubule gliding experiments were pursued to evaluate the effects of cross-linking restraints on Kar3Vik1 motility. The results show that Kar3Vik1 protein containing the same mutations as the 10- and 20-Å cross-linked GCN4-Kar3Vik1 but lacking disulfide bonds (non-cross-linked GCN4-Kar3Vik1) promoted microtubule minus-end–directed motility at 4.18 ± 0.03 μm/min (Fig. 6 C, Video 4, and Video 5). The 20-Å cross-linked GCN4-Kar3Vik1 promoted microtubule gliding at 4.26 ± 0.03 μm/min, which was indistinguishable from the motility promoted by the non-cross-linked GCN4-Kar3Vik1 (Videos 5 and 7). These cross-linking studies exclude interaction of the Kar3MD and Vik1MHD with αβ-tubulin subunits in a head–tail fashion on a single protofilament, as an ~80-Å separation of the heads is not required for binding of both heads to the microtubule.

Although Kar3 and Vik1 interact with adjacent protofilaments, the question remains: to what extent do the Kar3 and Vik1 motor heads separate during the motile cycle? Insight into this question is provided by the properties of the cross-linked motors.

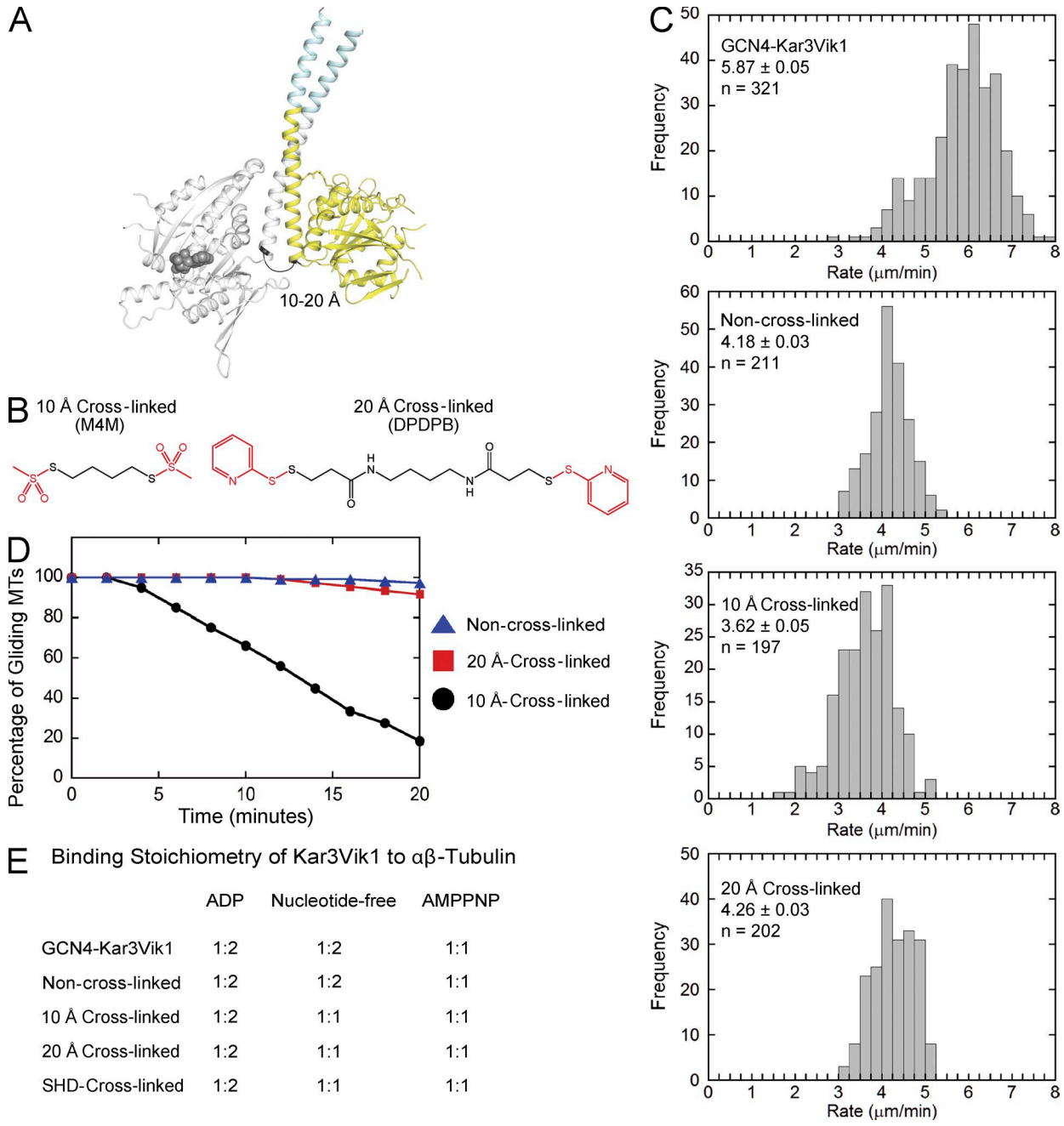

	ADP	Nucleotide-free	AMPPNP
GCN4-Kar3Vik1	1:2	1:2	1:1
Non-cross-linked	1:2	1:2	1:1
10 Å Cross-linked	1:2	1:1	1:1
20 Å Cross-linked	1:2	1:1	1:1
SHD-Cross-linked	1:2	1:1	1:1

Figure 6. **MT•Kar3Vik1 interactions upon neck coiled coil cross-linking.** (A) Model of Kar3Vik1 identifying the sites on Kar3 E382C and Vik1 K372C of the 10-Å and 20-Å cross-links. See Fig. S5 for cross-linking efficiency. (B) Chemical structures of M4M (10-Å cross-link) and DPDPB (20-Å cross-link). (C) Histograms of the velocity distribution of gliding microtubules for WT GCN4-Kar3Vik1, non-cross-linked, 10-Å cross-linked, and 20-Å cross-linked Kar3Vik1 motors. The rates are presented in 0.25 µm/min bins with the mean speed reported as mean ± SEM; *n* = number of microtubules scored. The data shown represent a total of 12–25 movies for each specific motor recorded on 3–6 different days. Representative movies are included as supplemental material. (D) Analysis of the persistence of motility promoted by non-cross-linked, 20-Å cross-linked, and 10-Å cross-linked GCN4-Kar3Vik1. Gliding microtubules were tracked for the initial 20 min of the experiments, and the percentage of microtubules that continued to move is presented: *n* = 110 microtubules for non-cross-linked, 110 microtubules for 20-Å cross-linked, and 221 microtubules for 10-Å cross-linked GCN4-Kar3Vik1. (E) MT•Kar3Vik1 cosedimentation to determine stoichiometry of binding. Gel images are not shown.

All motors display 1:2 stoichiometry of binding in the ADP state and 1:1 stoichiometry of binding in the AMPPNP state (Fig. 6). All motors exhibit minus-end–directed motility (Videos 1–7), and all motors display rotation of the coiled coil toward the minus end of the microtubule upon uptake of AMPPNP, as shown by cryo-EM (Fig. S4). This is regardless of whether they are cross-linked between Kar3 and Vik1's helix (10- and 20-Å cross-linked GCN4-Kar3Vik1) or cross-linked between Vik1's globular domain and helix (cross-linked SHD-Kar3Vik1), which suggests that only limited separation of the heads is required during the motile cycle.

In the nucleotide-free state, all cross-linked motors exhibit 1:1 stoichiometry of binding compared with 1:2 stoichiometry of binding exhibited for WT and non-cross-linked

constructs (Fig. 6 E). This change in binding does not appear critical to the motile cycle, as it does not abolish motility (Videos 1–7), but must reflect a subtle change in Kar3Vik1 binding in the nucleotide-free state compared with the ADP state, as only the nucleotide-free state appears sensitive to conformational restrictions within the heterodimer. Cryo-EM of cross-linked constructs suggests that during the nucleotide-free state, all motors are bound to microtubules through Kar3, similar to the nucleotide-free state observed for WT constructs in cryo-EM.

Unlike WT and 20-Å cross-linked GCN4-Kar3Vik1, 10-Å cross-linked GCN4-Kar3Vik1 promoted microtubule gliding initially at 3.62 ± 0.05 µm/min, but by 20 min, 80% of the microtubules stopped moving, with most microtubules detached from the coverslip and no longer visible in the field of view (Fig. 6 D and Video 6). It is hypothesized that 10-Å cross-linked GCN4-Kar3Vik1 was able to promote microtubule gliding initially because of the large number of Kar3Vik1 motors tethered to the coverslip and associated with the microtubules in this multiple motor assay. However, the 10-Å cross-link altered the normal simultaneous interactions of Kar3 and Vik1 with the microtubule lattice. Therefore, as a function of time, the microtubules may have either stalled binding predominantly by Vik1 or detached completely because of Kar3 reaching the ADP state.

Discussion

Kar3 and Vik1 directly participate in the motile cycle

Equilibrium binding of Kar3Vik1 in the ADP state unequivocally supports occlusion of two tubulin heterodimers by both the Kar3MD and Vik1MHD (Fig. 1). This does not answer the question of whether the heads bind along the same protofilament or on adjacent protofilaments, or whether both heads are tightly bound or one head is bound to and the other head is occluding a tubulin dimer. Successful binding of both heads to the microtubule, when cross-links have been introduced between the heads at the base of the coiled coil that restricts separation of the two globular domains, as shown by equilibrium binding, indirectly but strongly suggests binding of the heads to adjacent protofilaments (Fig. 6). This is further supported by unidirectionally surface-shadowed EM images of Kar3Vik1 in the ADP state (Fig. 2). However, the EM images of Kar3Vik1 in the ADP state alone are not sufficient to conclude adjacent protofilament binding, and it is only in combination with the cross-linked Kar3Vik1 equilibrium binding studies that this claim has been made. It is important to note that none of the data support binding of both heads along the same protofilament, nor is there any evidence within the literature that indicate binding along the same protofilament within the Kinesin-14 family. Additionally, this study does not represent an exhaustive study of this novel microtubule binding configuration, and further studies are needed to characterize how these heads interact with the microtubule.

This study presents the first direct evidence that a Kinesin-14 is able to have both heads bound to a microtubule during the motile cycle, and represents a novel kinesin microtubule binding configuration where heads are bound to adjacent protofilaments. Kar3 and Vik1 must bind to the microtubule in opposing orientations if the coiled coil does not unwind, as indicated by equilibrium binding of 10- and 20-Å cross-linked GCN4-Kar3Vik1 in the ADP state. This demands that Vik1 bind to microtubules in a different orientation than Kar3 or any other kinesin. Sequence and structural analyses support nonconventional binding of Vik1 to microtubules, as Vik1 shows no sequence conservation and significant structural differences in the region corresponding to the canonical kinesin microtubule-binding site. Previous equilibrium binding studies demonstrate that during the ADP state, the binding constant of Kar3Vik1 closely resembles that of the Vik1MHD, and that the Vik1MHD binds more tightly to the microtubule than the Kar3MD (Allingham et al., 2007). It seems likely that the Kar3Vik1 ADP state represents tight binding of Vik1 to the microtubule, with the Kar3 head weakly bound or released but occluding a tubulin binding site. This Kar3 binding state differs from the tightly bound intermediate observed in the nucleotide-free and AMPPNP states.

During the nucleotide-free state, two binding modes are observed. Equilibrium binding studies of WT GCN4-Kar3Vik1 show that both heads bind to the microtubule (Fig. 1), whereas cryo-EM of WT GCN4-Kar3Vik1 displays binding to the microtubule only through Kar3 (Fig. 4). The difference between the two experiments is due to the manner in which the complexes are assembled. Treatment of Kar3Vik1 with apyrase before binding to microtubules in equilibrium binding experiments results in ∼1:1 binding stoichiometry (Fig. 5), and favors cooperative nucleotide-free Kar3 binding to the microtubules as observed in EM (Cope et al., 2010). We predict that the equilibrium binding conditions in which Kar3Vik1 is first bound to microtubules with ADP and then treated with apyrase follow the sequence of events of binding and ADP release in vivo.

Equilibrium binding studies and cryo-EM both support binding of only Kar3 to the microtubule during the AMPPNP state (Figs. 1 and 4). Uptake of AMPPNP also leads to a rotation of the coiled coil toward the minus end of the microtubule as shown by cryo-EM (Fig. 4). The conformation of Kar3Vik1 in both the nucleotide-free and AMPPNP states closely resembles cryo-EM maps of Ncd, which suggests that this rotation is a general feature of the Kinesin-14 family. However, this rotation occurs only relative to Kar3, as Vik1 appears to rotate with the coiled coil. Thus, the question of whether the interface within the coiled coil and with Vik1 remains fixed or changes during the motile cycle can be raised.

Together, these experiments suggest a mechanism for Kar3Vik1 where Vik1 binds to the microtubule with Kar3 weakly bound in the ADP form on an adjacent protofilament. Release of ADP and uptake of ATP leads to dissociation of Vik1 and rotation of the coiled coil toward the minus end of the microtubule. This mechanism is summarized in Fig. 7.

Communication and conformation changes during the motile cycle

There must be communication between Kar3 and Vik1 such that Vik1 releases from the microtubule to allow motility. Unlike other kinesins, Vik1's microtubule binding affinity cannot be

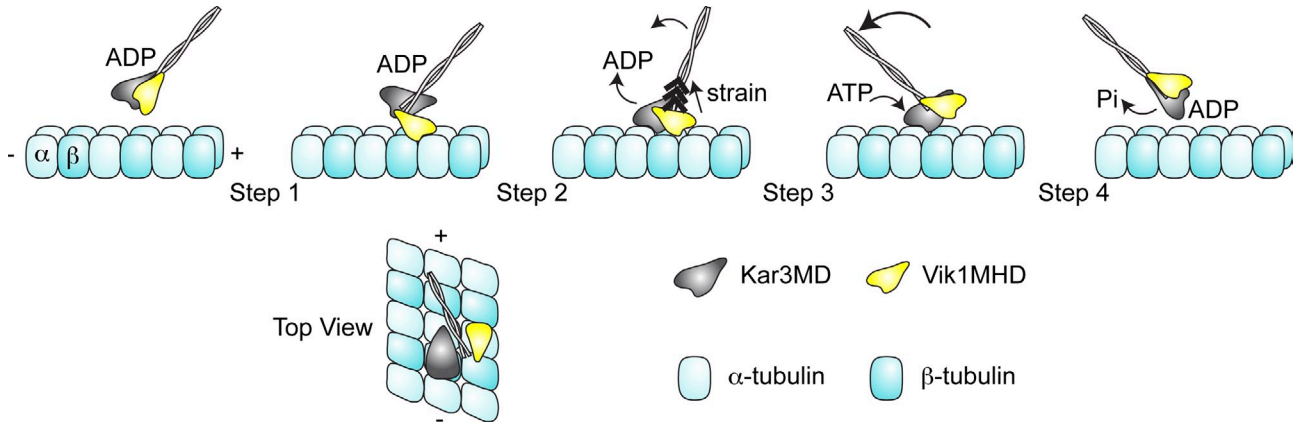

Figure 7. **Model of Kar3Vik1 mechanism of motion.** These schematic drawings present a model for Kar3Vik1 microtubule interaction during the motile cycle consistent with the experimental results presented here. In this mechanism, Vik1 binds first to the microtubule followed by Kar3 in the ADP form. Binding by Kar3 and release of ADP (Step 2) produces strain within the coiled coil, thereby weakening the affinity of Vik1 with the microtubule. ATP binding at Kar3 (Step 3) drives a large rotation of the coiled coil stalk toward the minus end of the microtubule. After ATP hydrolysis and P_i release (Step 4), the Kar3•ADP head detaches from the microtubule. Throughout the cycle, the coiled coil does not unwind significantly and imposes the restraint that Kar3 and Vik1 must bind to adjacent protofilaments where Vik1 cannot adopt a canonical microtubule-binding conformation on the lattice. Adapted from Allingham et al. (2007).

regulated by nucleotide binding and hydrolysis, yet it clearly changes during the motile cycle depending on the nucleotide state of Kar3. Therefore, there must be structural changes within Vik1 in response to the Kar3 nucleotide and microtubule binding state. There is no evidence in the Kar3Vik1 crystal structure of contact between the two heads except via the coiled coil (Fig. 3). However, the intermediate resolution cryo-EM structures may indicate some interaction (Fig. 4). This implies that communication at the early stages of the motile cycle, as represented by the x-ray structure, may occur through conformational changes associated with the coiled coil itself.

Equilibrium binding and motility studies of Kar3Vik1 motors cross-linked at the base of the helix suggest that some limited separation of the coiled coil is necessary for function because the stoichiometry of the nucleotide state changes from 1:2 to 1:1. The necessity for conformational freedom is further supported by the changes in motility introduced by the 10-Å cross-link. Together, these observations imply conformational changes within Kar3Vik1 during nucleotide release. Additional higher-resolution structures of Kar3Vik1 during different states of the motile cycle will be needed to further elucidate the structural mechanism by which binding to microtubules and hydrolysis of ATP transmits conformational changes between the globular domains of Kar3 and Vik1.

Evolutionary conservation of the second Kinesin-14 head suggests functional importance. The experiments presented here demonstrate that in Kar3Vik1, the second head directly participates in the motile cycle. What then is the functional value of Vik1 microtubule binding? It is conceivable that Vik1 plays a role in coordination and processivity of an ensemble of motors. Alternatively, Vik1 may function to orient Kar3 for more rapid binding to microtubules, promote correct assembly of the motor ensemble, or increase the likelihood of rebinding to microtubules after dissociation. Questions concerning communication and function await further investigation.

Materials and methods

Cloning

All cloning was performed as described previously (Klenchin et al., 2011). In brief, a modified QuikChange mutagenesis protocol was used to introduce all point mutants, and QuikChange cloning was used to amplify and insert the Kar3 and Vik1 genes. All constructs generated were sequence verified over the entire open reading frame insert.

Constructs

All Kar3 constructs were amplified from *S. cerevisiae* genomic DNA and introduced into a modified pET24d (EMD) plasmid by QuikChange cloning. Vik1 constructs were also amplified from *S. cerevisiae* genomic DNA and introduced into a Strep II tag version of pKLD37, a modified pET31b plasmid (EMD), by QuikChange cloning (Rocco et al., 2008). Construct designs are listed in Table 1.

Preparation of the streptavidin column

A mutant streptavidin optimized to bind the Strep II tag was purified as described previously (Schmidt and Skerra, 1994; Voss and Skerra, 1997). In brief, native streptavidin was expressed as inclusion bodies in an *Escherichia coli* BL21-CodonPlus (DE3)-RIL cell line (Agilent Technologies). Inclusion bodies were solubilized in 6 M guanidine × HCl, pH 1.5, and protein was refolded by rapid dilution into 75 mM Hepes, pH 7.5, with 100 mM NaCl. Folded streptavidin was then concentrated by precipitation in an 80% saturated ammonium sulfate solution at 4°C, resuspended in Milli-Q water, and dialyzed against Milli-Q water to remove remaining ammonium sulfate. Protein was lyophilized and stored at −20°C.

Streptavidin was coupled to Sepharose CL-4B using periodate activation (Sanderson and Wilson, 1971; Wilson and Nakane, 1976). Sepharose CL-4B (Pharmacia) was activated by adding two column volumes of 20 mg/ml $NaIO_4$ and allowed to react with gentle mixing for 2 h at room temperature. The activated Sepharose was washed with 10 column volumes of Milli-Q water and equilibrated in carbonate buffer (100 mM Na_2CO_3, pH 10.5). Purified streptavidin was added to a final concentration of 5 mg streptavidin per milliliter of activated Sepharose and allowed to couple for 16 h at room temperature with gentle mixing. The protein-coupled Sepharose was then washed with two column volumes of carbonate buffer. One column volume of freshly prepared 3 mg/ml $NaBH_4$ in carbonate buffer was added and allowed to react with gentle mixing at room temperature for 5 min. The column was then washed with 10 column volumes of carbonate buffer and equilibrated in a suitable buffer for protein purification. Protocol courtesy of V.V. Sinitsyn.

Protein expression and purification

Kar3 and Vik1 plasmids were coexpressed in an *E. coli* BL21-CodonPlus (DE3)-RIL cell line (Stratagene). Cells were grown in lysogeny broth (LB)

medium to an A_{600} of ~0.9, then cooled on ice for 15 min; at this point, 0.5 mM IPTG was added and the cells were grown for 16 h at 16°C with shaking before harvesting by centrifugation. The Kar3Vik1 heterodimers were purified as follows; all procedures were performed at 4°C. 20 g of cell paste in 200 ml of lysis buffer (20 mM Tris, pH 8.0, 300 mM NaCl, 30 mM imidazole, 2 mM $MgCl_2$, 0.1 mM EGTA, 0.5 mM TCEP, and 0.2 mM ATP) with 1 mM PMSF, 50 nM Leupeptin (Peptide International), 70 nM E-65 (Peptide International), 2 nM Aprotinin (ProSpec), and 2 µM AEBSF (Gold BioTechnology) were lysed by sonication and centrifuged at 125,000 *g* for 30 min at 4°C. The supernatant was loaded onto a 7 ml Ni-NTA column (QIAGEN) at a rate of 1 ml/min and washed with 15 column volumes of lysis buffer. Protein was eluted in four column volumes of elution buffer (lysis buffer with 200 mM imidazole). The elution from the Ni-NTA column was directly loaded onto a 50-ml streptavidin agarose column at a rate of 2 ml/min, washed with three column volumes of wash buffer (20 mM Tris buffer, 300 mM NaCl, 2 mM $MgCl_2$, 0.1 mM EGTA, 0.5 mM TCEP, and 0.2 mM ATP), and eluted in three column volumes wash buffer with 2.5 mM Desthiobiotin.

The octa-Histidine and Strep II tag were removed by incubation with a 1:40 molar ratio of rTEV protease to Kar3Vik1 for 16 h at 4°C for proteins used in crystallization and EM studies (Blommel and Fox, 2007). The cleaved protein was then loaded onto a 2-ml Ni-NTA column equilibrated in rTEV buffer (20 mM Tris, pH 8.0, 300 mM NaCl, 2 mM $MgCl_2$, 0.1 mM EGTA, 0.5 mM TCEP, and 0.2 mM ATP); Kar3Vik1 was eluted in three column volumes of rTEV buffer with 30 mM imidazole, and rTEV was eluted with rTEV buffer with 200 mM imidazole. All protein constructs were concentrated in a Centriprep YM-50 (Millipore) to 10–15 mg/ml. Proteins for crystallization and EM were dialyzed into 20 mM Tris, pH 8.0, 100 mM NaCl, 2 mM $MgCl_2$, 1 mM EGTA, 0.2 mM ATP, and 0.5 mM TCEP, then frozen as 30-µl drops into liquid nitrogen and stored at −80°C.

Protein cross-linking

All procedures were performed at 4°C. Concentrated protein was exchanged into cross-linking buffer (20 mM Tris, pH 8.0, 150 mM NaCl, 2 mM $MgCl_2$, 1 mM EGTA, and 0.2 mM ATP degassed and then sparged with Argon) using a PD-10 column (Pharmacia). A 10-fold molar excess of M4M, EBI (Toronto Research Company), or DPDPB (Thermo Fisher Scientific) was immediately added and allowed to react with stirring for 30 min (or 16 h in the dark for EBI). After cross-linking, protein was concentrated to 10–15 mg/ml and dialyzed into 20 mM Tris, pH 8.0, 100 mM NaCl, 2 mM $MgCl_2$, 1 mM EGTA, and 0.2 mM ATP.

Crystallization of cross-linked SHD-Kar3Vik1

Crystals were grown by small-scale batch crystallization, where 4 µl of concentrated protein was mixed with 5 µl PEG solution (16% monomethyl polyethylene glycol 2000, 100 mM Hepes, pH 7.5, and 50 mM sodium citrate; Rayment, 2002). Drops were immediately streak-seeded, then allowed to grow at 4°C for 3 wk. Crystals grew to maximal dimensions of 1 mm × 100 µm × 100 µm. For freezing, crystals were transferred to a synthetic mother liquor (12% monomethyl polyethylene glycol 5000, 75 mM Hepes, pH 7.5, 37.5 mM sodium citrate, 5 mM Tris, pH 8.0, 25 mM NaCl, 0.5 mM $MgCl_2$, 0.25 mM EGTA, and 80 µM ATP) and then transferred stepwise to a solution of 18% polyethylene glycol 8000, 16% glycerol, 100 mM Hepes, pH 7.5, 0.2 mM ATP, 2 mM $MgCl_2$, and 250 mM sodium citrate. Crystals were flash-frozen in liquid nitrogen.

X-ray data collection and structural refinement

X-ray diffraction data for the cross-linked SHD-Kar3Vik1 crystals were collected at the SBC 19-ID beam line (Advanced Photon Source). The datasets were integrated and scaled with the program HKL2000 (Otwinowski and Minor, 1997). X-ray data collection statistics are given in Table 2. The structure of Kar3Vik1 was solved by molecular replacement using the program Phaser (Collaborative Computational Project 4, 1994; McCoy et al., 2007) and the structure with PDB accession nos. 3KAR and 2O0A as the search models (Gulick et al., 1998; Allingham et al., 2007). Parrot was used for density modification, and these phases were used to build an initial model in Buccaneer (Cowtan, 2008, 2010). This was followed by iterative cycles of manual model building in Coot and restrained and TLS refinement in Refmac 5.6 (Emsley and Cowtan, 2004; Skubák et al., 2004). Data processing and refinement statistics are presented in Table 2. All structural alignments were done with the program Superpose using secondary structure matching (Krissinel and Henrick, 2004).

High-resolution metal shadowing

Decoration of microtubules with dimeric Kar3Vik1 was performed after adsorbing microtubules to plain, glow-discharged carbon grids for 1 min in the presence of 10 mM ADP. The initial solution of microtubules during absorption to EM grids was at 0.4 mg/ml, but excess liquid was briefly blotted away from the grids before adding 4 µl of a solution of Kar3Vik1 at 0.8 mg/ml. The microtubules that remained on the grids were incubated with the motor solution for 10 min. Then excess liquid was again blotted away from the grids, which were immediately plunged into liquid nitrogen for rapid freezing. The frozen grids were freeze-dried for 90 min in the so-called Midilab system (a unique freeze-drying/metal shadowing unit located at the Eidgenössische Technische Hochschule Zürich, Hoenggerberg, Switzerland), and subsequently shadowed unidirectionally with a 3–4-Å-thick layer of tantalum-tungsten at an elevation angle of 45° (Hoenger and Gross, 2008).

Table 2. **Crystal structure data collection and refinement statistics**

Criteria	Cross-linked SHD-Kar3Vik1
Space group	$P2_12_12_1$
Cell dimensions	
a, *b*, *c* (Å)	88.1, 94.9, 114.6
α, β, γ (°)	90, 90, 90
Wavelength	0.979206
Resolution (Å)[a]	25–2.3 (2.34–2.3)
R_{merge}[a]	5.1 (60.1)
$I/\sigma I$[a]	19.7 (3.2)
Completeness (%)[a]	99.9 (99.8)
Redundancy[a]	8.6 (6.2)
Resolution (Å)[a]	25–2.3 (2.34–2.3)
No. reflections[b]	40710 (2701)
R_{work}/R_{free}[c]	0.21/0.24
No. atoms	
Protein	5361
Water	246
Average *B*-factors (Å^2)	
Protein	69.991
Water	54.972
R.m.s. deviations	
Bond lengths (Å)	0.005
Bond angles (°)	0.891
PDB accession no.	4ETP

[a]Data in parentheses represent the highest resolution shell.
[b]Data in parentheses represent the number of reflections used for the calculation of R_{free}.
[c]$R_{factor} = \Sigma||F_{obs}|-|F_{calc}|| \,/\, \Sigma|F_{obs}|$.
Where R_{work} refers to the R_{factor} for the data utilized in the refinement and R_{free} refers to the R_{factor} for 5% of the data that were excluded from the refinement.

Microtubule polymerization for cryo-EM studies

Microtubules were polymerized in vitro from purified bovine brain tubulin (Cytoskeleton) with 80 mM Pipes, pH 6.8, 1 mM $MgCl_2$, 1 mM EGTA, 1 mM GTP, 10 µM paclitaxel, and 8% DMSO for 30 min at 37°C, then allowed to stabilize overnight at room temperature (Cope et al., 2010).

Vitrification of MT•Kar3Vik1 for cryo-EM

MT•Kar3Vik1 complexes were assembled directly on holey carbon C-flat grids (Protochips) to prevent microtubules from bundling. Polymerized microtubules at 3.75 µM were adsorbed to a holey carbon grid for 35–60 s. Excess liquid was blotted away, and 5 µl of 5–8 µM Kar3Vik1 in the appropriate nucleotide state was immediately added to the microtubules for 90–120 s before blotting away excess liquid and plunging the grid into liquid ethane using a homemade plunge-freezing device. To achieve the nucleotide-free state, Kar3Vik1 was incubated on ice with 1 U of apyrase grade VII (Sigma-Aldrich) for 30–45 min. To mimic the ATP state, Kar3Vik1 was incubated on ice with the ATP analogue AMPPNP (Sigma-Aldrich) for 10–30 min.

Cryo-EM data collection and helical reconstruction

Plunge-frozen samples were transferred under liquid nitrogen to a Gatan-626 cryo-holder (Gatan). Two-dimensional projections of vitreously frozen MT•Kar3Vik1 complexes were acquired on an FEI Tecnai F20 FEG transmission electron microscope (FEI Company) operating at 200 kV. Single-frame images were taken at a nominal magnification of 29,000× and a defocus of −2.5 µm

with a total electron dose of 15 electrons/Å^2. Images were recorded without binning on a 4,000 × 4,000 charge-coupled device camera (Ultrascan 895; Gatan) with the resulting pixel size corresponding to 3.8 Å on the specimen.

Helical processing was performed using PHOELIX essentially as described previously (Whittaker et al., 1995). In brief, each microtubule was computationally straightened, and layer-line information was extracted. Layer-line data from a large number of microtubules were shifted to a common phase origin using a reference and subsequently averaged. IMOD (Kremer et al., 1996) and UCSF Chimera (Pettersen et al., 2004) were used for visualization and surface rendering of the electron density maps of the averages.

The number of individual datasets and approximate number of asymmetric units included in each of the helical reconstructions is shown in Fig. S3.

Docking of crystal structures into cryo-EM maps

The crystal structure of the αβ-tubulin dimer (PDB accession no. 1JFF; Löwe et al., 2001) was docked manually into the electron density maps using UCSF Chimera (Pettersen et al., 2004). The Kar3Vik1 heterodimer crystal structure (PDB accession no. 4ETP) was docked initially into the maps manually using Chimera by positioning Kar3 onto the microtubule based on the results of Hirose et al. (2006). The Kar3Vik1 crystal structure was then docked quantitatively into the map of the nucleotide-free state using the FFT-Accelerated 6D Exhaustive Search tool in Situs (Chacón and Wriggers, 2002). This program was used to perform a rigid-body, exhaustive search around translational and rotational space to obtain the best global fit of Kar3Vik1 into the electron density map. The fit that gave the highest correlation score from this quantitative docking was in very close agreement with our initial manual docking result. To dock Kar3Vik1 into the AMPPNP state maps, the structure was divided into two rigid-body components that could be manipulated separately: (1) the Kar3MD core (residues G385-K729) and (2) the complete Vik1MHD domain with the coiled coil stalk. Each component was docked interactively by eye into the maps to obtain the best fit.

MT•Kar3Vik1 cosedimentation assays

Reactions of 200 µl were formed with 2 µM Kar3Vik1 plus microtubules (0–10 µM tubulin polymer and 40 µM paclitaxel in ATPase buffer: 20 mM Hepes, pH 7.2, with KOH, 5 mM magnesium acetate, 0.1 mM EDTA, 0.1 mM EGTA, 50 mM potassium acetate, 1 mM dithiothreitol, and 5% sucrose) in the presence of either 1 mM MgADP, 1 mM MgAMPPNP, or 100 µM MgADP followed by apyrase treatment (0.02 U/ml, grade VII; Sigma-Aldrich) to generate the nucleotide-free state as described previously (Chen et al., 2011). The samples were incubated at room temperature for 30 min followed by centrifugation. The supernatant and pellet for each reaction were analyzed by SDS-PAGE, followed by Coomassie Blue staining. To determine the fraction of Kar3Vik1 that partitions to the pellet, the gels were scanned, and ImageJ (National Institutes of Health) was used to convert the scanned image to a TIFF file. Image Gauge version 4 software (FUJIFILM Science Laboratory) was used to box the Kar3Vik1 gel bands as a unit for conversion to pixel number. A box of comparable size was used to obtain a background sample. The background total was subtracted from each Kar3Vik1 sample. For each microtubule concentration, the Image Gauge sum for Kar3Vik1 partitioning to the pellet was divided by the sum of the Kar3Vik1 in the supernatant + pellet, thereby providing the fraction. Note that each sample is independent of the others, with supernatant + pellet = 100% of 2 µM Kar3Vik1. This approach avoids errors associated with small differences in loading volumes. The fraction of Kar3Vik1 that partitioned with the microtubule pellet as a function of microtubule concentration was plotted, and the data were fit to the following quadratic equation because of the stoichiometric binding conditions of the experiment: $[(MT•E)/(E)] = 0.5 \times \{(E_0 + K_d + MT_0) - [(E_0 + K_d + MT_0)^2 - (4E_0MT_0)]^{1/2}\}$. MT•E/E is the fraction of Kar3Vik1 that partitioned with the microtubules, E_0 is total Kar3Vik1, K_d is the apparent dissociation constant, and MT_0 is the microtubule concentration. Fig. 1 shows representative experiments at each condition. Each experiment was repeated multiple times with the K_d constants reported as the mean ± SEM.

Polarity marked microtubules and microtubule gliding assay

Polarity marked paclitaxel-stabilized rhodamine-labeled microtubules were assembled, and the motility assays were performed as described previously (Allingham et al., 2007; Sardar et al., 2010). Before each experiment, Kar3Vik1 was clarified and the protein concentration was determined by the Bio-Rad Protein assay (IgG as standard). Protein concentrations are expressed as the Kar3Vik1 heterodimer concentration with one nucleotide binding site per Kar3Vik1.

The MT•Kar3Vik1 complex (1 µM Kar3Vik1, 0.5 µM polarity marked rhodamine-microtubules, and 20 µM paclitaxel) was preformed in the presence of 0.5 mM MgAMPPNP in ATPase buffer: 20 mM Hepes, pH 7.2, with KOH, 5 mM magnesium acetate, 0.1 mM EDTA, 0.1 mM EGTA, 50 mM potassium acetate, 1 mM dithiothreitol, and 5% sucrose. The microscope perfusion chamber was rinsed with PME-80 buffer (80 mM Pipes, pH 6.9, with KOH, 5 mM $MgCl_2$, and 1 mM EGTA) and coated with Penta-His antibodies (QIAGEN) at 100 µg/ml, followed by a blocking buffer containing 1 mM MgAMPPNP and an oxygen scavenger mix (OSM; 1× PME-80 buffer, 1 mg/ml casein, 0.2 mg/ml glucose oxidase, 0.175 mg/ml catalase, 25 mM glucose, and 20 µM paclitaxel). The MT•Kar3Vik1•AMPPNP complex was then perfused into the chamber and became immobilized to the slide by the N-terminal His tag of Kar3Vik1 bound to the Penta-His antibodies. After a 5-min incubation, PME-80 + 0.5 mM MgAMPPNP buffer wash was flowed into the chamber to remove unbound microtubules and motors. microtubule gliding was initiated by adding 1.5 mM MgATP with an ATP regeneration system (0.3 µg/µl creatine phosphokinase and 2 mM phosphocreatine in OSM buffer). The final mix was: 1× PME-80 buffer, 1.5 mM ATP, 1.5 mM magnesium acetate, 0.2 mg/ml glucose oxidase, 0.175 mg/ml catalase, 25 mM glucose, 0.5% β-mercaptoethanol, and 20 µM paclitaxel. Note that reducing agents (DTT, β-mercaptoethanol) were excluded from the buffers and reaction mix for experiments with cross-linked Kar3Vik1 motors.

Total internal reflection fluorescence (TIRF) microscopy was used to visualize movement of polarity-marked rhodamine microtubules at 25°C. Imaging was performed on an AxioObserver Z1 Inverted Laser TIRF3 microscope system (Carl Zeiss) using the TIRF DsRed filter set. Images were recorded with the electron multiplier (EM-CCD) digital camera (Hamamatsu Photonics) using the 100×/1.46 α-Plan-Apochromat oil objective lens. The Definite Focus module (Carl Zeiss) was used to stabilize image capture. Images were collected every 20 s for 45 min with an exposure time of 180 ms. All movies and images were analyzed and processed with the AxioVision Release 4.8.2 software and Photoshop (Adobe). microtubules that were scored met the following criteria: microtubules were entirely within the field of view, were ≥ 3 µm but ≤ 8 µm in length, and travelled in a clearly defined path. Because the Kar3Vik1 motors were immobilized on the coverslip, microtubule minus-end–directed motility is observed with the bright microtubule minus end trailing with the dimmer microtubule plus end leading.

Steady-state ATPase kinetics

The turnover of α-[^{32}P]ATP to α-[^{32}P]ADP•P_i during steady-state was determined in ATPase buffer as described previously (Gilbert and Mackey, 2000). These experiments were performed by preparing two tubes, each with 50 µl for a total reaction volume of 100 µl. The Kar3Vik1 tube A contained the specific Kar3Vik1 motor, microtubules, ATPase buffer, and 40 µM paclitaxel. The ATP tube B contained 1 µl of α-[^{32}P]ATP, unlabeled MgATP, and ATPase buffer. The reactions were initiated by the addition of 5 µl of tube A to 5 µl of tube B and incubated at 25°C for varying times (eight time points per 100-µl reaction). At each time point, the 10-µl reaction was terminated by the addition of 20 µl of 10 N formic acid. The zero time points were determined by denaturing the Kar3Vik1 (5 µl of tube A) with 20 µl formic acid before mixing with 5 µl of tube B. An aliquot (1 µl) of the terminated reaction mixture for each time point was spotted onto a polyethyleneimine cellulose F TLC plate (20 × 20 cm, plastic-backed; EM Science) and developed in 0.6 M potassium phosphate buffer, pH 3.4, with phosphoric acid to separate the products α-[^{32}P]ADP + P_i from α-[^{32}P]ATP. Each TLC plate was scanned, and the radiolabeled nucleotide was quantified using Image Gauge V4.0 software (Fujifilm) to box the α-[^{32}P]ADP and α-[^{32}P]ATP spots for conversion to pixel number.

For each time point, the sum of ADP divided by the sum of ADP + ATP provided the fraction of ATP that was hydrolyzed during the time of the reaction. This fraction is converted to micromolar ADP formed at each time point based on the ATP concentration in the reaction and corrected for the contaminating α-[^{32}P]ADP using the zero time point data. The ADP product formed was plotted as a function of time, and the linear fit of each time course provided the observed rate of the reaction (micromolar ADP produced per Kar3Vik1 per second) for each ATP concentration. The observed rates (s^{-1}) plotted as a function of increasing MgATP concentration were fit to the Michaelis-Menten equation, and the microtubule concentration dependence data were fit to the following quadratic equation because the enzyme concentration was not 10-fold less than the $K_{1/2,MT}$. $\text{Rate} = 0.5 \times k_{cat} \times \{(E_0 + K_{1/2,MT} + MT_0) - [(E_0 + K_{1/2,MT} + MT_0)^2 - (4E_0S_0)]^{1/2}\}$. The rate is the product of ADP•Pi formed per second per Kar3Vik1 active site, k_{cat} is the maximum rate constant of steady-state turnover at saturating

microtubules, E_0 is the Kar3Vik1 concentration in (μM), $K_{1/2,MT}$ is the concentration of tubulin polymer that yields half the k_{cat}, and MT_0 is the tubulin polymer concentration (μM).

Online supplemental material

Fig. S1 elaborates on the Kar3Vik1 construct design. Fig. S2 displays motor properties of GCN4-Kar3Vik1 and SHD-Kar3Vik1. Fig. S3 confirms the registration of Kar3Vik1's coiled coil within the x-ray crystal structure. Fig. S4 presents the cryo-EM and helical reconstructions of cross-linked Kar3Vik1. Fig. S5 demonstrates the cross-linking efficiency of cross-linked Kar3Vik1 motors. Videos 1–7 show the motility of WT SHD-Kar3Vik1, non-cross-linked SHD-Kar3Vik1, cross-linked SHD-Kar3Vik1, WT GCN4-Kar3Vik1, non-cross-linked GCN4-Kar3Vik1, 10-Å cross-linked Kar3Vik1, and 20-Å cross-linked Kar3Vik1, respectively. Online supplemental material is available at http://www.jcb.org/cgi/content/full/jcb.201201132/DC1.

We thank John Allingham for his work on the initial GCN4-Kar3Vik1 constructs, Soheila Vaezeslami for her work on the GCN4-Kar3Vik1 constructs and removal of the cysteines from Kar3 and Vik1, Martin St. Maurice for his work on the initial cross-linked constructs, Dima Klenchin for his suggestion of using the SHD fusion construct and for technical assistance, Emily Ross for the initial motility analysis of the M4M cross-linked motors, and Peter Tittmann (Eidgenössische Technische Hochschule Zürich Hoenggerberg) for his help with high-resolution metal shadowing.

This work was supported by grants from the National Institutes of Health to I. Rayment (GM086351), S.P. Gilbert (GM54141), and A. Hoenger (P41-RR000592). K.C. Rank and J. Cope were both supported by NIH training grants (T32-GM07215 and T32-GM065103, respectively). Use of the Structural Biology ID19 beamline, Argonne National Laboratory Advanced Photon Source was supported by the U.S. Department of Energy, Office of Energy Research, under Contract No. W-31-109-ENG-38.

Submitted: 24 January 2012
Accepted: 15 May 2012

References

Allingham, J.S., L.R. Sproul, I. Rayment, and S.P. Gilbert. 2007. Vik1 modulates microtubule-Kar3 interactions through a motor domain that lacks an active site. *Cell*. 128:1161–1172. http://dx.doi.org/10.1016/j.cell.2006.12.046

Asbury, C.L., A.N. Fehr, and S.M. Block. 2003. Kinesin moves by an asymmetric hand-over-hand mechanism. *Science*. 302:2130–2134. http://dx.doi.org/10.1126/science.1092985

Barrett, J.G., B.D. Manning, and M. Snyder. 2000. The Kar3p kinesin-related protein forms a novel heterodimeric structure with its associated protein Cik1p. *Mol. Biol. Cell*. 11:2373–2385.

Blommel, P.G., and B.G. Fox. 2007. A combined approach to improving large-scale production of tobacco etch virus protease. *Protein Expr. Purif.* 55:53–68. http://dx.doi.org/10.1016/j.pep.2007.04.013

Chacón, P., and W. Wriggers. 2002. Multi-resolution contour-based fitting of macromolecular structures. *J. Mol. Biol.* 317:375–384. http://dx.doi.org/10.1006/jmbi.2002.5438

Chen, C.J., I. Rayment, and S.P. Gilbert. 2011. Kinesin Kar3Cik1 ATPase pathway for microtubule cross-linking. *J. Biol. Chem.* 286:29261–29272. http://dx.doi.org/10.1074/jbc.M111.255554

Chu, H.M., M. Yun, D.E. Anderson, H. Sage, H.W. Park, and S.A. Endow. 2005. Kar3 interaction with Cik1 alters motor structure and function. *EMBO J.* 24:3214–3223. http://dx.doi.org/10.1038/sj.emboj.7600790

Clancy, B.E., W.M. Behnke-Parks, J.O. Andreasson, S.S. Rosenfeld, and S.M. Block. 2011. A universal pathway for kinesin stepping. *Nat. Struct. Mol. Biol.* 18:1020–1027. http://dx.doi.org/10.1038/nsmb.2104

Collaborative Computational Project 4. 1994. The CCP4 Suite: Programs for protein crystallography. *Acta Crystallogr.* D50:760–763.

Cope, J., S. Gilbert, I. Rayment, D. Mastronarde, and A. Hoenger. 2010. Cryo-electron tomography of microtubule-kinesin motor complexes. *J. Struct. Biol.* 170:257–265. http://dx.doi.org/10.1016/j.jsb.2009.12.004

Cowtan, K. 2008. Fitting molecular fragments into electron density. *Acta Crystallogr. D Biol. Crystallogr.* 64:83–89. http://dx.doi.org/10.1107/S0907444907033938

Cowtan, K. 2010. Recent developments in classical density modification. *Acta Crystallogr. D Biol. Crystallogr.* 66:470–478. http://dx.doi.org/10.1107/S090744490903947X

deCastro, M.J., R.M. Fondecave, L.A. Clarke, C.F. Schmidt, and R.J. Stewart. 2000. Working strokes by single molecules of the kinesin-related microtubule motor ncd. *Nat. Cell Biol.* 2:724–729. http://dx.doi.org/10.1038/35036357

Emsley, P., and K. Cowtan. 2004. Coot: model-building tools for molecular graphics. *Acta Crystallogr. D Biol. Crystallogr.* 60:2126–2132. http://dx.doi.org/10.1107/S0907444904019158

Endres, N.F., C. Yoshioka, R.A. Milligan, and R.D. Vale. 2006. A lever-arm rotation drives motility of the minus-end-directed kinesin Ncd. *Nature*. 439:875–878. http://dx.doi.org/10.1038/nature04320

Fink, G., L. Hajdo, K.J. Skowronek, C. Reuther, A.A. Kasprzak, and S. Diez. 2009. The mitotic kinesin-14 Ncd drives directional microtubule-microtubule sliding. *Nat. Cell Biol.* 11:717–723. http://dx.doi.org/10.1038/ncb1877

Foster, K.A., and S.P. Gilbert. 2000. Kinetic studies of dimeric Ncd: evidence that Ncd is not processive. *Biochemistry*. 39:1784–1791. http://dx.doi.org/10.1021/bi991500b

Foster, K.A., J.J. Correia, and S.P. Gilbert. 1998. Equilibrium binding studies of non-claret disjunctional protein (Ncd) reveal cooperative interactions between the motor domains. *J. Biol. Chem.* 273:35307–35318. http://dx.doi.org/10.1074/jbc.273.52.35307

Foster, K.A., A.T. Mackey, and S.P. Gilbert. 2001. A mechanistic model for Ncd directionality. *J. Biol. Chem.* 276:19259–19266. http://dx.doi.org/10.1074/jbc.M008347200

Gardner, M.K., J. Haase, K. Mythreye, J.N. Molk, M. Anderson, A.P. Joglekar, E.T. O'Toole, M. Winey, E.D. Salmon, D.J. Odde, and K. Bloom. 2008. The microtubule-based motor Kar3 and plus end-binding protein Bim1 provide structural support for the anaphase spindle. *J. Cell Biol.* 180:91–100. http://dx.doi.org/10.1083/jcb.200710164

Gilbert, S.P., and A.T. Mackey. 2000. Kinetics: a tool to study molecular motors. *Methods*. 22:337–354. http://dx.doi.org/10.1006/meth.2000.1086

Gulick, A.M., H. Song, S.A. Endow, and I. Rayment. 1998. X-ray crystal structure of the yeast Kar3 motor domain complexed with Mg.ADP to 2.3 A resolution. *Biochemistry*. 37:1769–1776. http://dx.doi.org/10.1021/bi972504o

Hackney, D.D. 1994. Evidence for alternating head catalysis by kinesin during microtubule-stimulated ATP hydrolysis. *Proc. Natl. Acad. Sci. USA*. 91:6865–6869. http://dx.doi.org/10.1073/pnas.91.15.6865

Hancock, W.O., and J. Howard. 1999. Kinesin's processivity results from mechanical and chemical coordination between the ATP hydrolysis cycles of the two motor domains. *Proc. Natl. Acad. Sci. USA*. 96:13147–13152. http://dx.doi.org/10.1073/pnas.96.23.13147

Heuston, E., C.E. Bronner, F.J. Kull, and S.A. Endow. 2010. A kinesin motor in a force-producing conformation. *BMC Struct. Biol.* 10:19. http://dx.doi.org/10.1186/1472-6807-10-19

Hildebrandt, E.R., and M.A. Hoyt. 2000. Mitotic motors in *Saccharomyces cerevisiae*. *Biochim. Biophys. Acta*. 1496:99–116. http://dx.doi.org/10.1016/S0167-4889(00)00012-4

Hirose, K., R.A. Cross, and L.A. Amos. 1998. Nucleotide-dependent structural changes in dimeric NCD molecules complexed to microtubules. *J. Mol. Biol.* 278:389–400. http://dx.doi.org/10.1006/jmbi.1998.1709

Hirose, K., E. Akimaru, T. Akiba, S.A. Endow, and L.A. Amos. 2006. Large conformational changes in a kinesin motor catalyzed by interaction with microtubules. *Mol. Cell*. 23:913–923. http://dx.doi.org/10.1016/j.molcel.2006.07.020

Hoenger, A., and H. Gross. 2008. Structural investigations into microtubule-MAP complexes. *Methods Cell Biol.* 84:425–444. http://dx.doi.org/10.1016/S0091-679X(07)84014-3

Hoenger, A., S. Sack, M. Thormählen, A. Marx, J. Müller, H. Gross, and E. Mandelkow. 1998. Image reconstructions of microtubules decorated with monomeric and dimeric kinesins: comparison with x-ray structure and implications for motility. *J. Cell Biol.* 141:419–430. http://dx.doi.org/10.1083/jcb.141.2.419

Kaseda, K., H. Higuchi, and K. Hirose. 2003. Alternate fast and slow stepping of a heterodimeric kinesin molecule. *Nat. Cell Biol.* 5:1079–1082. http://dx.doi.org/10.1038/ncb1067

Klenchin, V.A., J.J. Frye, M.H. Jones, M. Winey, and I. Rayment. 2011. Structure-function analysis of the C-terminal domain of CNM67, a core component of the *Saccharomyces cerevisiae* spindle pole body. *J. Biol. Chem.* 286:18240–18250. http://dx.doi.org/10.1074/jbc.M111.227371

Kocik, E., K.J. Skowronek, and A.A. Kasprzak. 2009. Interactions between subunits in heterodimeric Ncd molecules. *J. Biol. Chem.* 284:35735–35745. http://dx.doi.org/10.1074/jbc.M109.024240

Kremer, J.R., D.N. Mastronarde, and J.R. McIntosh. 1996. Computer visualization of three-dimensional image data using IMOD. *J. Struct. Biol.* 116:71–76. http://dx.doi.org/10.1006/jsbi.1996.0013

Krissinel, E., and K. Henrick. 2004. Secondary-structure matching (SSM), a new tool for fast protein structure alignment in three dimensions. *Acta Crystallogr. D Biol. Crystallogr.* 60:2256–2268. http://dx.doi.org/10.1107/S0907444904026460

Krzysiak, T.C., T. Wendt, L.R. Sproul, P. Tittmann, H. Gross, S.P. Gilbert, and A. Hoenger. 2006. A structural model for monastrol inhibition of dimeric

kinesin Eg5. *EMBO J.* 25:2263–2273. http://dx.doi.org/10.1038/sj.emboj.7601108

Lindhout, D.A., J.R. Litowski, P. Mercier, R.S. Hodges, and B.D. Sykes. 2004. NMR solution structure of a highly stable de novo heterodimeric coiled-coil. *Biopolymers*. 75:367–375. http://dx.doi.org/10.1002/bip.20150

Löwe, J., H. Li, K.H. Downing, and E. Nogales. 2001. Refined structure of alpha beta-tubulin at 3.5 A resolution. *J. Mol. Biol.* 313:1045–1057. http://dx.doi.org/10.1006/jmbi.2001.5077

Maddox, P.S., J.K. Stemple, L. Satterwhite, E.D. Salmon, and K. Bloom. 2003. The minus end-directed motor Kar3 is required for coupling dynamic microtubule plus ends to the cortical shmoo tip in budding yeast. *Curr. Biol.* 13:1423–1428. http://dx.doi.org/10.1016/S0960-9822(03)00547-5

Manning, B.D., J.G. Barrett, J.A. Wallace, H. Granok, and M. Snyder. 1999. Differential regulation of the Kar3p kinesin-related protein by two associated proteins, Cik1p and Vik1p. *J. Cell Biol.* 144:1219–1233. http://dx.doi.org/10.1083/jcb.144.6.1219

McCoy, A.J., R.W. Grosse-Kunstleve, P.D. Adams, M.D. Winn, L.C. Storoni, and R.J. Read. 2007. Phaser crystallographic software. *J. Appl. Cryst.* 40:658–674. http://dx.doi.org/10.1107/S0021889807021206

Meluh, P.B., and M.D. Rose. 1990. KAR3, a kinesin-related gene required for yeast nuclear fusion. *Cell.* 60:1029–1041. http://dx.doi.org/10.1016/0092-8674(90)90351-E

Molk, J.N., E.D. Salmon, and K. Bloom. 2006. Nuclear congression is driven by cytoplasmic microtubule plus end interactions in *S. cerevisiae. J. Cell Biol.* 172:27–39. http://dx.doi.org/10.1083/jcb.200510032

O'Shea, E.K., J.D. Klemm, P.S. Kim, and T. Alber. 1991. X-ray structure of the GCN4 leucine zipper, a two-stranded, parallel coiled coil. *Science*. 254:539–544. http://dx.doi.org/10.1126/science.1948029

Otwinowski, Z., and W. Minor. 1997. Processing of X-ray diffraction data collected in oscillation mode. *Methods Enzymol.* 276:307–326. http://dx.doi.org/10.1016/S0076-6879(97)76066-X

Page, B.D., and M. Snyder. 1992. CIK1: a developmentally regulated spindle pole body-associated protein important for microtubule functions in *Saccharomyces cerevisiae. Genes Dev.* 6:1414–1429. http://dx.doi.org/10.1101/gad.6.8.1414

Page, B.D., L.L. Satterwhite, M.D. Rose, and M. Snyder. 1994. Localization of the Kar3 kinesin heavy chain-related protein requires the Cik1 interacting protein. *J. Cell Biol.* 124:507–519. http://dx.doi.org/10.1083/jcb.124.4.507

Pettersen, E.F., T.D. Goddard, C.C. Huang, G.S. Couch, D.M. Greenblatt, E.C. Meng, and T.E. Ferrin. 2004. UCSF Chimera—a visualization system for exploratory research and analysis. *J. Comput. Chem.* 25:1605–1612. http://dx.doi.org/10.1002/jcc.20084

Rayment, I. 2002. Small-scale batch crystallization of proteins revisited: an underutilized way to grow large protein crystals. *Structure*. 10:147–151. http://dx.doi.org/10.1016/S0969-2126(02)00711-6

Rice, S., A.W. Lin, D. Safer, C.L. Hart, N. Naber, B.O. Carragher, S.M. Cain, E. Pechatnikova, E.M. Wilson-Kubalek, M. Whittaker, et al. 1999. A structural change in the kinesin motor protein that drives motility. *Nature*. 402:778–784. http://dx.doi.org/10.1038/45483

Rocco, C.J., K.L. Dennison, V.A. Klenchin, I. Rayment, and J.C. Escalante-Semerena. 2008. Construction and use of new cloning vectors for the rapid isolation of recombinant proteins from *Escherichia coli. Plasmid*. 59:231–237. http://dx.doi.org/10.1016/j.plasmid.2008.01.001

Sablin, E.P., R.B. Case, S.C. Dai, C.L. Hart, A. Ruby, R.D. Vale, and R.J. Fletterick. 1998. Direction determination in the minus-end-directed kinesin motor ncd. *Nature*. 395:813–816. http://dx.doi.org/10.1038/27463

Sanderson, C.J., and D.V. Wilson. 1971. A simple method for coupling proteins to insoluble polysaccharides. *Immunology*. 20:1061–1065.

Sardar, H.S., V.G. Luczak, M.M. Lopez, B.C. Lister, and S.P. Gilbert. 2010. Mitotic kinesin CENP-E promotes microtubule plus-end elongation. *Curr. Biol.* 20:1648–1653. http://dx.doi.org/10.1016/j.cub.2010.08.001

Schmidt, T.G., and A. Skerra. 1994. One-step affinity purification of bacterially produced proteins by means of the "Strep tag" and immobilized recombinant core streptavidin. *J. Chromatogr. A*. 676:337–345. http://dx.doi.org/10.1016/0021-9673(94)80434-6

Skiniotis, G., T. Surrey, S. Altmann, H. Gross, Y.H. Song, E. Mandelkow, and A. Hoenger. 2003. Nucleotide-induced conformations in the neck region of dimeric kinesin. *EMBO J.* 22:1518–1528. http://dx.doi.org/10.1093/emboj/cdg164

Skubák, P., G.N. Murshudov, and N.S. Pannu. 2004. Direct incorporation of experimental phase information in model refinement. *Acta Crystallogr. D Biol. Crystallogr.* 60:2196–2201. http://dx.doi.org/10.1107/S0907444904019079

Sosa, H., D.P. Dias, A. Hoenger, M. Whittaker, E. Wilson-Kubalek, E. Sablin, R.J. Fletterick, R.D. Vale, and R.A. Milligan. 1997. A model for the microtubule-Ncd motor protein complex obtained by cryo-electron microscopy and image analysis. *Cell*. 90:217–224. http://dx.doi.org/10.1016/S0092-8674(00)80330-X

Sproul, L.R., D.J. Anderson, A.T. Mackey, W.S. Saunders, and S.P. Gilbert. 2005. Cik1 targets the minus-end kinesin depolymerase kar3 to microtubule plus ends. *Curr. Biol.* 15:1420–1427. http://dx.doi.org/10.1016/j.cub.2005.06.066

Svoboda, K., C.F. Schmidt, B.J. Schnapp, and S.M. Block. 1993. Direct observation of kinesin stepping by optical trapping interferometry. *Nature*. 365:721–727. http://dx.doi.org/10.1038/365721a0

Vale, R.D., and R.J. Fletterick. 1997. The design plan of kinesin motors. *Annu. Rev. Cell Dev. Biol.* 13:745–777. http://dx.doi.org/10.1146/annurev.cellbio.13.1.745

Voss, S., and A. Skerra. 1997. Mutagenesis of a flexible loop in streptavidin leads to higher affinity for the Strep-tag II peptide and improved performance in recombinant protein purification. *Protein Eng.* 10:975–982. http://dx.doi.org/10.1093/protein/10.8.975

Wendt, T.G., N. Volkmann, G. Skiniotis, K.N. Goldie, J. Müller, E. Mandelkow, and A. Hoenger. 2002. Microscopic evidence for a minus-end-directed power stroke in the kinesin motor ncd. *EMBO J.* 21:5969–5978. http://dx.doi.org/10.1093/emboj/cdf622

Whittaker, M., B.O. Carragher, and R.A. Milligan. 1995. PHOELIX: a package for semi-automated helical reconstruction. *Ultramicroscopy*. 58:245–259. http://dx.doi.org/10.1016/0304-3991(95)00057-8

Wilson, M.B., and P.K. Nakane. 1976. The covalent coupling of proteins to periodate-oxidized sephadex: a new approach to immunoadsorbent preparation. *J. Immunol. Methods*. 12:171–181. http://dx.doi.org/10.1016/0022-1759(76)90107-1

Yildiz, A., M. Tomishige, R.D. Vale, and P.R. Selvin. 2004. Kinesin walks hand-over-hand. *Science*. 303:676–678. http://dx.doi.org/10.1126/science.1093753

Yildiz, A., M. Tomishige, A. Gennerich, and R.D. Vale. 2008. Intramolecular strain coordinates kinesin stepping behavior along microtubules. *Cell*. 134:1030–1041. http://dx.doi.org/10.1016/j.cell.2008.07.018

Yun, M., C.E. Bronner, C.G. Park, S.S. Cha, H.W. Park, and S.A. Endow. 2003. Rotation of the stalk/neck and one head in a new crystal structure of the kinesin motor protein, Ncd. *EMBO J.* 22:5382–5389. http://dx.doi.org/10.1093/emboj/cdg531